Supplement of Atmos. Chem. Phys., 23, 6963–6988, 2023
https://doi.org/10.5194/acp-23-6963-2023-supplement

Supplement of

A 1-year aerosol chemical speciation monitor (ACSM) source analysis of organic aerosol particle contributions from anthropogenic sources after long-range transport at the TROPOS research station Melpitz

Samira Atabakhsh et al.

Correspondence to: Hartmut Herrmann (herrmann@tropos.de)

1 Source apportionment of organic aerosol

This work conducted the most advanced source apportionment analysis following a standardized protocol developed by Chen et al., (2022). In this study, to better identify the organic aerosol (OA) sources in Melpitz, positive matrix factorization (PMF) was applied on each separate season, following a standardized protocol developed by Chen et al., (2022). Since the measurements were taken between September 2016 and August 2017 (12 months), therefore dataset was split into four meteorological seasons (i.e., fall (September-November); winter (December-February); spring (March-May), and summer (June-August)). Details of the rolling PMF can be found in Chen et al., (2022).

1.1 PMF pre-test

First, to estimate the potential sources in different seasons, unconstrained PMF was applied with different factors (from 4 to 6) runs on each season separately. Considering the residential heating during winter time, it was estimated to have the maximum coal combustion OA (CCOA) and biomass burning OA (BBOA) emissions in this season. Therefore, in order to identify and split the sources of solid fuels, the winter season was comprehensively analyzed. However, clear primary factor profiles did not result from unconstrained PMF during the winter season. Therefore, profiles of two primary factors as hydrocarbon-like OA (HOA) and BBOA were constrained by various *a-values* and applying the reference profiles by Crippa et. Al. (2013) and Ng et al. (2011a) for HOA and BBOA, respectively as suggested by Chen et al. (2021). After HOA and BBOA constraining, a third primary factor could be dedicated as well. This new primary factor presented signals which are common in CCOA profiles (e.g., signals from unsaturated hydrocarbons and polycyclic aromatic hydrocarbons (PAHs)). The bootstrap resampling strategy was applied to the input data matrix to check the reliability of the discovered CCOA factor (Davison and Hinkley, 1997). Three primary factors (HOA, BBOA, and resulted CCOA) were used to constrain the PMF solution. Finally, based on residual analysis, it was possible to determine the number of oxygenated OA (OOA). When the number of factors was increased to 6 or more, either the OOAs or the CCOA were split. As a result, throughout the measurements, the five-factor solution with three primary factors and two OOA factors was preferred. $\mu g\ m^{-3}$

PMF with the rolling window approach was performed based on these seasonal pre-tests. The following section describes the specific settings used in this study. Since this approach resulted in an immense number of single PMF solutions, it was necessary to identify and distinguish environmentally reasonable PMF solutions, by using properly selected user-defined criteria. The unconstrained factors were also identified and sorted using these criteria. The particular details of the factors are discussed further below.

The correlation of NO_x with HOA factor is used as a HOA criterion since it is known as a typical tracer for traffic emissions. However, to determine if the difference in this correlation was considerable in comparison with the correlation of NO_x with other factors, a *t-test* was performed that solutions with a *p-value* ≤ 0.05 were considered acceptable for all the criteria. For the BBOA factor, the explained variation of *m/z* 60 was selected as a criterion, since BBOA is typically composed of anhydrous sugar fragments (e.g., levoglucosan fragments *m/z* 60 and 73). Moreover, the correlation of levoglucosan with BBOA was used as the second criterion for this factor. For the CCOA factor, unsaturated hydrocarbon and polycyclic aromatic hydrocarbon (PAH) signals at *m/z* 41, 51, 53, 55, 69, 77, 91, and 115 characterize coal combustion emissions (Dall'Osto et al., 2013; Elser et al., 2016; Lin et al., 2017; Xu et al., 2020). Therefore, as a CCOA criterion, the explained variation of *m/z* 115 was selected. Further, the R^2 value of the time series of POA factors (HOA, BBOA, and CCOA) vs equivalent black carbon (eBC-PM_1) was used for them as other criteria. The unconstrained OOA factors were split by less oxidized oxygenated OA (LO-OOA) and more oxidized oxygenated OA (MO-OOA). We used f_{44} for the MO-OOA as suggested by (Chen et al., 2021) which LO-OOA simply followed by f_{43}.

1.2 Rolling PMF

Following the analysis of the seasonal PMF solutions (i.e., pre-test PMF), rolling PMF was carried out. The shift parameter (the number of days), the width of the window (the number of consecutive days), and the number of repetitions for each PMF window define the rolling PMF approach (Canonaco et al., 2021). Here, to detect source variation, the PMF window with a length of 14 days with a 1-day shift was applied as suggested by (Chen et al., 2021). To compare the four different PMF analyses, the same criteria and thresholds have been used.

To investigate the statistical uncertainties of the rolling PMF, repeats per window are needed. However, statistical uncertainty could be evaluated by using the bootstrap strategy, which resamples the PMF input at random. When the factors are constrained by prior knowledge (i.e., reference profiles or external time series), a sensitivity analysis of the *a-value* must be done to investigate the rotational ambiguity. The *a-values* in this study were selected at random for each PMF repetition, ranging from 0 to 0.4 for HOA and BBOA, and 0.5 for CCOA (Δa = 0.1 for all). Based on the criteria described above, 15165 solutions (42.36 %) of the overall 35800 single PMF runs were produced in the rolling PMF approach. All measured time points were modeled within the context of a rolling PMF. As presented in Fig. S1, no systematic errors were observed during the evaluation of the scaled residual over time and variables (*m/z*). The uncertainty is described as the logarithmic probability density function (pdf) of the standard deviation of each time point *i* divided by the mean mass concentration of each time point *i*. As time points with a low signal-to-noise ratio would pull the error calculations, the lognormal distribution was chosen to better represent the PMF errors. As shown in Fig. S2, the relative PMF errors are ± 32.5 %, ± 27.6 %, ± 28.9 %, ± 38.2 % and ± 24.4 % for HOA, BBOA, CCOA, LO-OOA and MO-OOA, respectively.

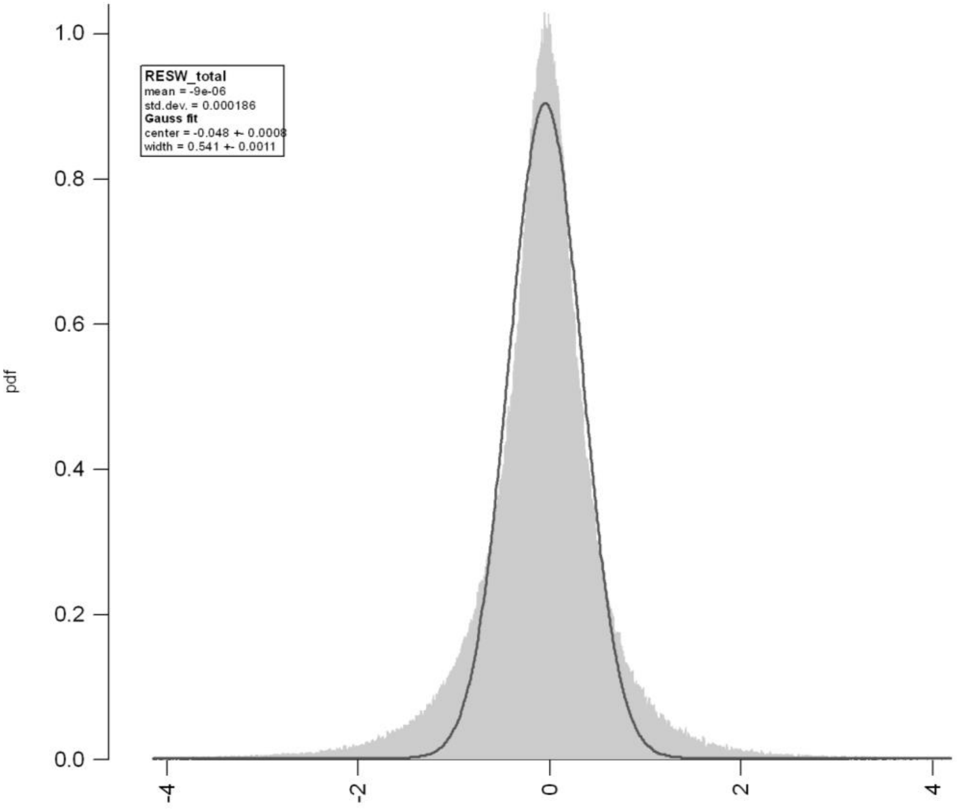

Fig. S1: Analysis of the scaled residuals for the total scaled residuals.

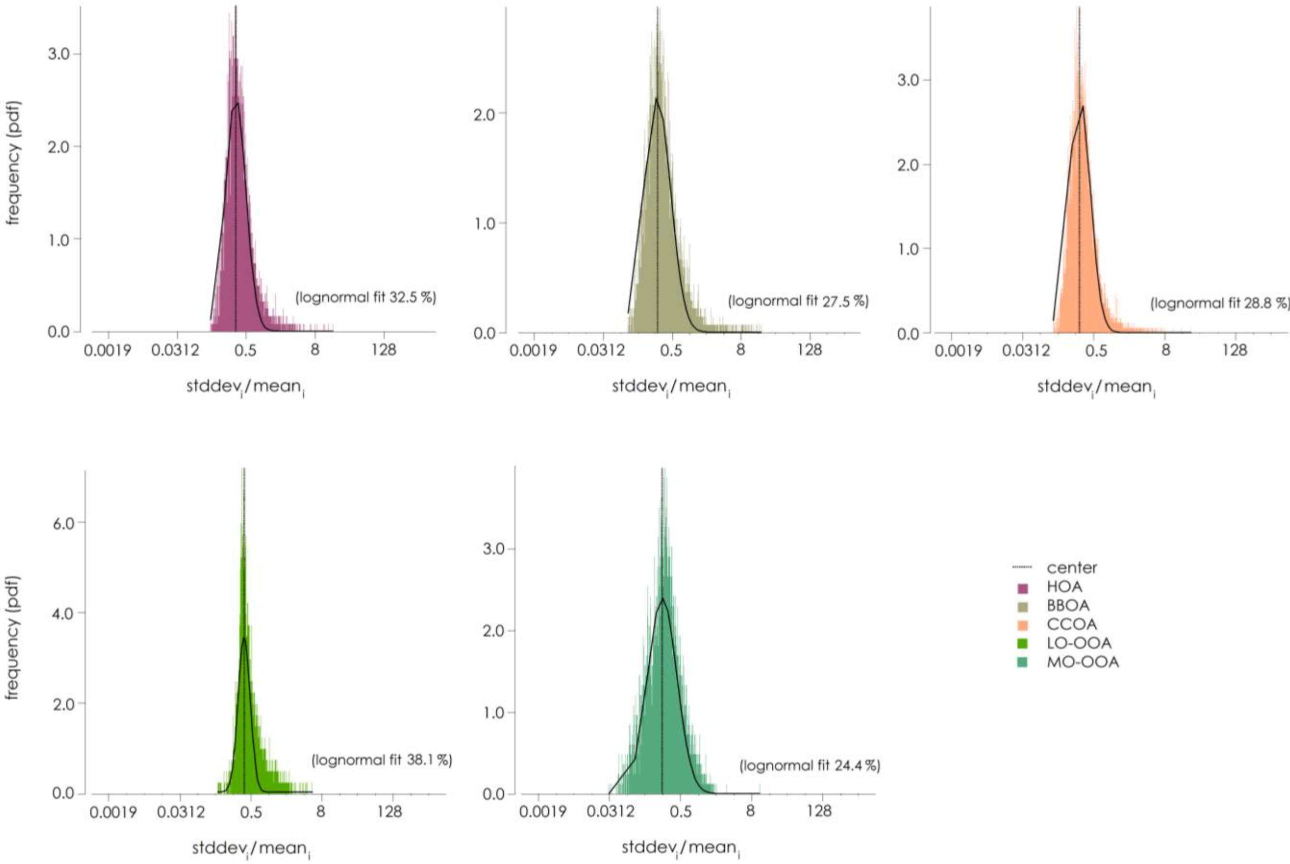

Fig. S2: PMF error estimation of the five resolved PMF factors represented as logarithmic probability density functions (pdf) of the standard deviations of each time point *i* divided by the mean mass concentration of each time point *i*.

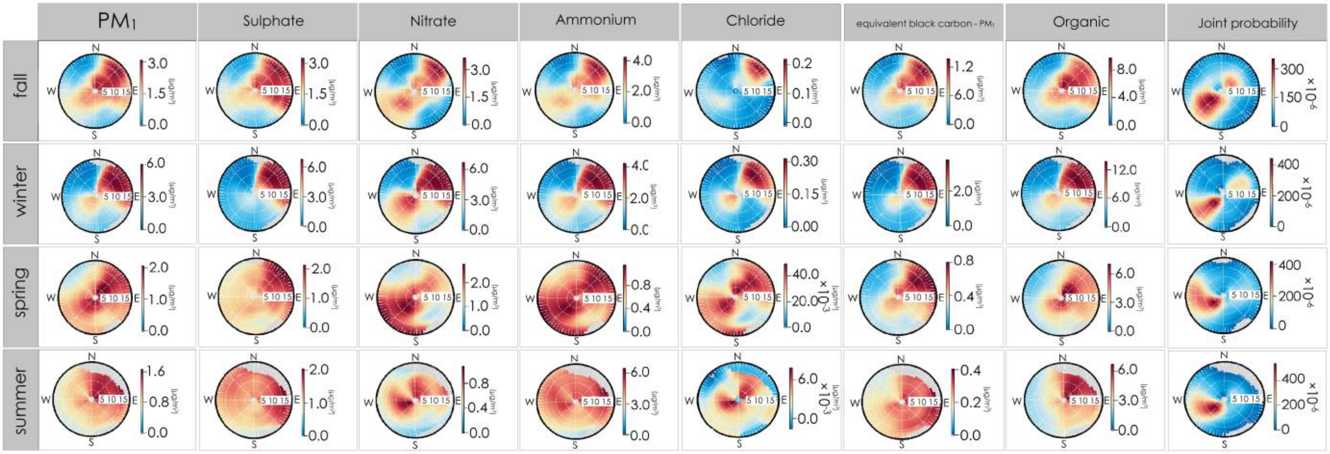

Fig. S3: Seasonal NWR plots for the different chemical compositions (in μg m^{-3}). PM$_1$ is the average of all the compositions.

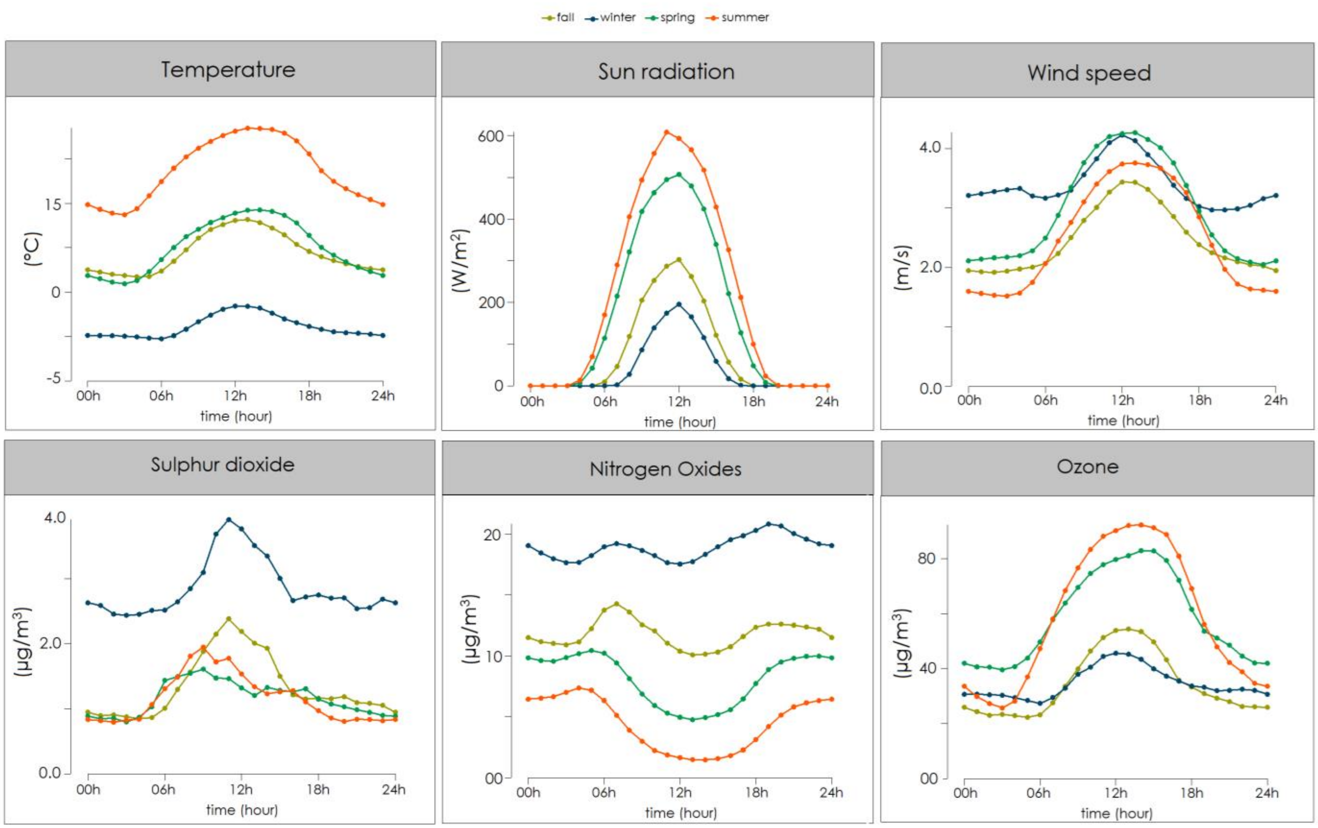

Fig. S4: Seasonal diurnal cycle of Temperature, Sun radiation, Sulphur dioxide, Nitrogen Oxides, and Ozone.

Table. S1: PM_1 seasonal mass fraction (%) of each ACSM species, and AMS study (Poulain et al, 2011).

	Species	Fall		Winter		Summer	
		ACSM	AMS	ACSM	AMS	ACSM	AMS
ACSM	Org	50	32	39	23	58	59
	SO_4^{2-}	16	17	15	18	20	22
	NO_3^-	18	23	24	34	11	5
	NH_4^+	9	12	12	17	7	8
	Cl^-	0	0	1	2	0	0
MAAP	eBC-PM_1	6	10	9	6	4	6

Table. S2: PM_1 seasonal mass concentration ($\mu g\ m^{-3}$) of Poulain et al, (2020), and average from the current study.

Species	**Fall**	**Winter**	**Summer**	**Spring**	**Average**	**the current study**
Org	3.83	4.58	4.41	4.28	4.27	4.84
SO_4^2-	1.53	1.86	1.37	1.41	1.54	1.67
NO3-	2.24	3.79	0.90	3.07	2.50	2.16
NH_4^+	1.10	1.63	0.65	1.35	1.18	1.11
Cl-	0.04	0.07	0.01	0.05	0.04	0.05
eBC-PM_1	0.69	1.22	0.30	0.56	0.69	0.66
Tot	9.43	13.15	7.64	10.72	10.23	10.49

Table. S3: Studies information: Current study, Crippa et al., 2014, van Pinxteren et al., 2016 and 2020.

Information	**Current study**	Crippa et al., 2014	van Pinxteren et al., 2016	van Pinxteren et al., 2020
Instrument	ACSM	AMS	Berner-type cascade impactor	Digitel DHA-80 high-volume filter samplers
PM size	1 µm	1 µm	0.05, 0.14, 0.42, 1.2, 3.5, and 10 µm	10 µm
PM type	Organic	Organic	Total mass	Total mass
Data coverage	1 year (Sep 2016-Aug2017)	2 spring, 1 fall	21 days per: 1 summer, 1 winter	1 year (Nov2018- Oct2019)
Sources category	HOA, BBOA, CCOA, LO-OOA, MO-OOA	HOA, BBOA, LO-OOA, MO-OOA	Crustal material, Salt, Secondary I, II, Biomass combustion, Coal combustion	Traffic, Tr. Exhaust, CCOA, BBOA, SA, Photochem, Cooking, Spores, Urban dust, Sea salt

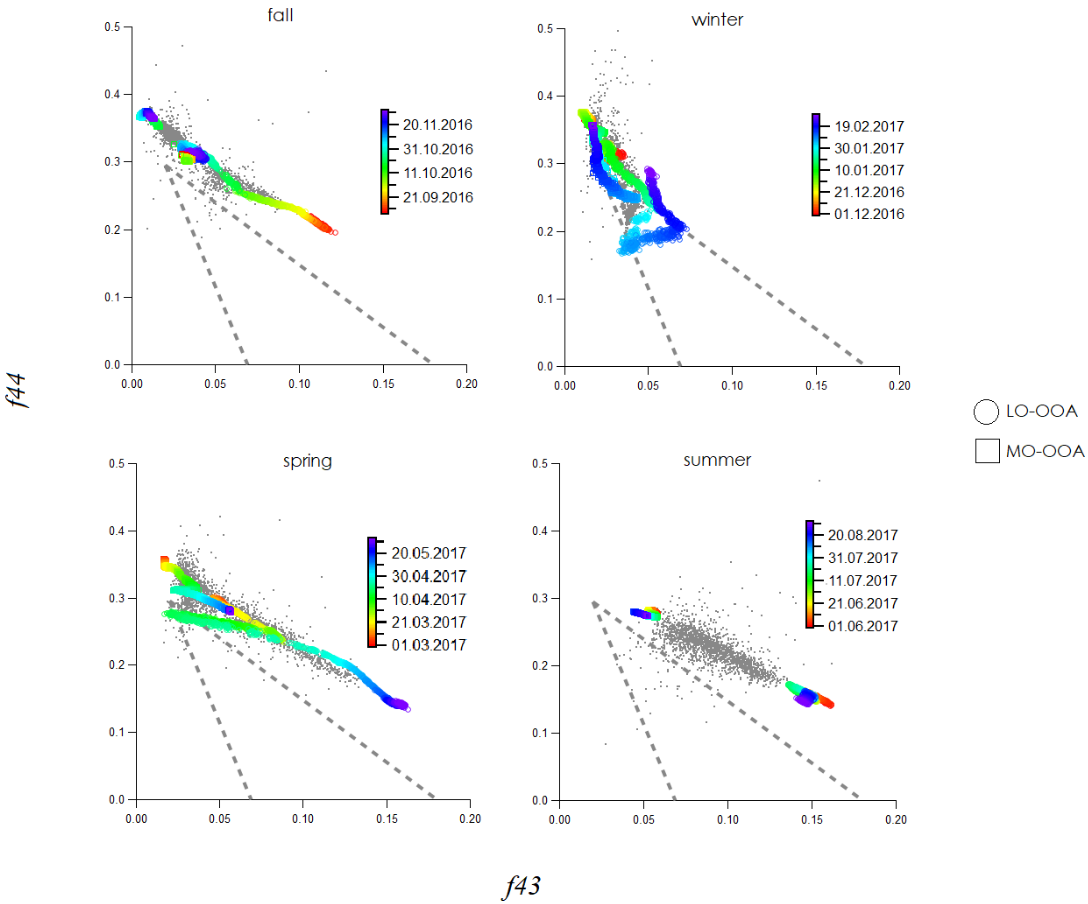

Fig. S5: *f44* vs. *f43* for OOA factors (after subtraction of signals contributed by the primary HOA, BBOA, and CCOA factors as shown in Eq. (S1) and (S2)) in hourly resolution, colour coded by date. The triangle plot established by Ng et al., (2010), depicts the region where several PMF OOA from the last decade resided in the *f44* vs *f43* space

$$subtracted\ f44 = \frac{mass\ conc.of\ OOA\ @\ [m/z44]}{mass\ conc.of\ OOA + residual\ of\ total\ OA} \quad \text{(S1)}$$

$$subtracted\ f43 = \frac{mass\ conc.of\ OOA\ @\ [m/z43]}{mass\ conc.of\ OOA + residual\ of\ total\ OA} \quad \text{(S2)}$$

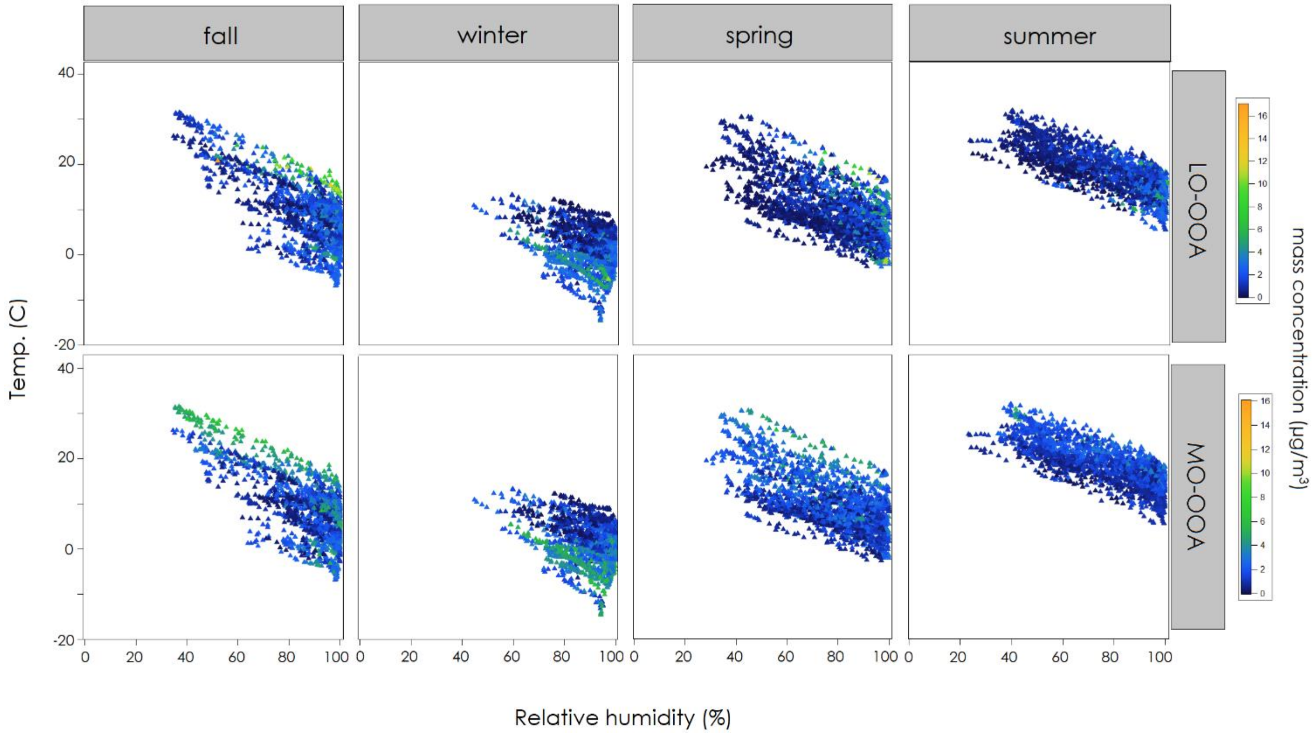

Fig. S6: Temperature (T) and relative humidity (RH) dependence variations of the mass loadings of two OOA fractions.

Table. S4: Linear regression coefficient for m_{HOA}, m_{BBOA}, and m_{CCOA}, defined as a, b, and c for HOA, BBOA, and CCOA; respectively.

Factor	**Fall**	**Winter**	**Spring**	**Summer**
a (HOA)	0.38	0.55	0.11	0.17
b (BBOA)	0.95	0.52	0.65	0.75
c (CCOA)	0.32	0.46	0.35	0.09

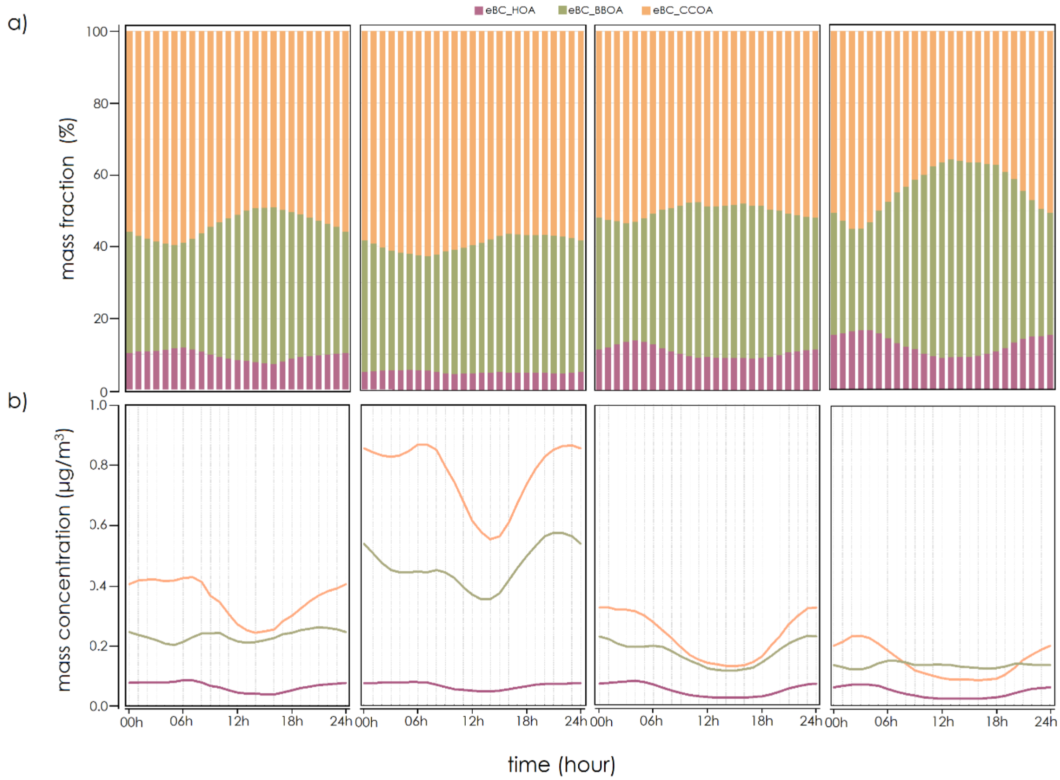

Fig. S7: The diurnal variation of different eBC-PM$_1$, a) mass fraction, b) mass concentration of the POA for different seasons.

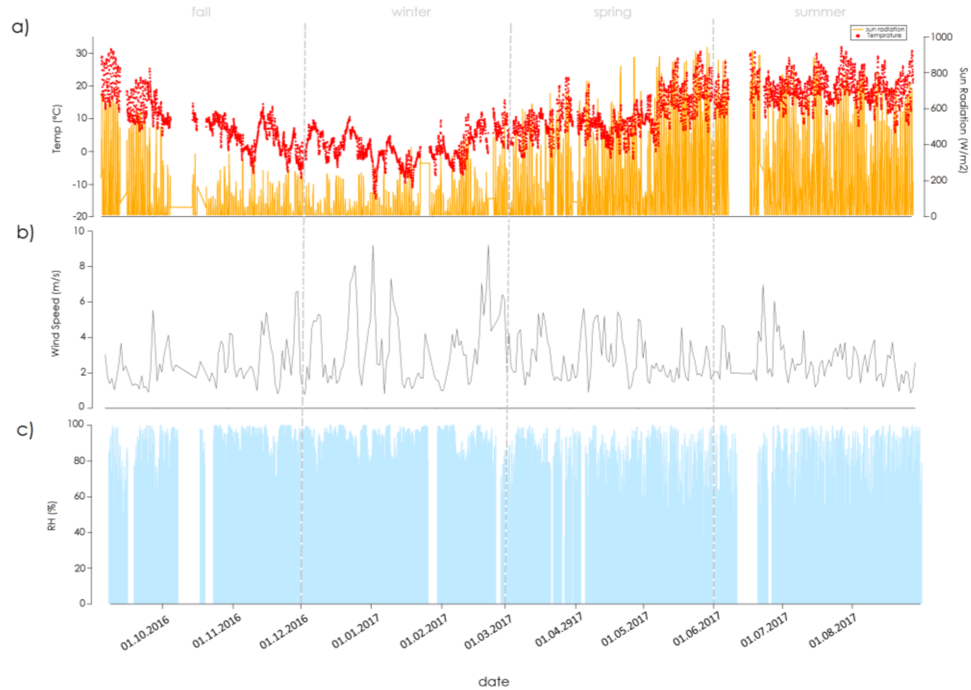

Fig. S8: Time series of meteorological variables; a) hourly resolution of Temperature in red dots, Sun radiation in yellow line, b) daily resolution of Wind speed and c) hourly resolution of Relative Humidity (time is in UTC).

Table. S5: Main statistical details of the fifteen air mass types for PM_1 and PMF factors (CS=Cold Season, WS=Warm Season, ST=Stagnant, A=Anticyclonic, C=Cyclonic) based on mass concentration (μg m^{-3}).

Main season	Airmass type	Wind direction	Vorticity	Average mass concentration (μg/m^3)											
				eBC-HOA	eBC-BBOA	eBC-CCOA	NO_3^-	SO_4^{-2}	NH_4^+	Cl^-	HOA	BBOA	CCOA	LO_OOA	MO_OOA
Winter	CS-ST	Stagnating	Anticyclonic	0.06	0.62	0.91	5.38	3.33	2.78	0.14	0.35	0.97	1.89	2.73	2.73
	CS-A1	East	Anticyclonic	0.08	0.67	1.93	5.60	5.39	3.44	0.24	0.49	1.06	4.01	2.72	3.45
	CS-A2	West	Anticyclonic	0.04	0.24	0.31	3.86	1.83	1.89	0.13	0.25	0.38	0.65	1.77	1.97
	CS-C1	South	Cyclonic	0.05	0.38	0.40	2.62	2.99	1.75	0.06	0.30	0.61	0.84	2.17	3.77
	CS-C2a	South West	Cyclonic	0.01	0.07	0.06	1.16	0.78	0.58	0.03	0.07	0.11	0.13	0.30	0.72
	CS-C2b	West	Cyclonic	0.01	0.04	0.05	0.35	0.74	0.26	0.02	0.07	0.07	0.10	0.29	0.55
Transition (Spring/ Fall)	TS-A1	North East	Anticyclonic	0.03	0.11	0.13	1.08	1.07	0.59	0.04	0.17	0.17	0.27	1.03	1.31
	TS-A2	West	Anticyclonic	0.02	0.09	0.08	1.54	1.05	0.73	0.03	0.11	0.15	0.18	0.60	1.23
	TS-C1	South West	Cyclonic	0.02	0.12	0.15	0.77	0.68	0.36	0.01	0.15	0.19	0.31	0.65	1.24
	TS-C2	North West	Cyclonic	0.01	0.07	0.08	1.35	0.90	0.68	0.06	0.09	0.12	0.18	0.50	0.84
Summer	WS-ST	Stagnating	Anticyclonic	0.04	0.21	0.17	1.01	1.88	0.71	0.01	0.23	0.34	0.36	1.10	2.84
	WS-A1	South East	Anticyclonic	0.06	0.32	0.62	3.20	3.25	1.96	0.10	0.34	0.51	1.28	2.15	3.11
	WS-A2	North West	Anticyclonic	0.03	0.14	0.21	2.22	1.63	1.09	0.04	0.19	0.23	0.44	1.13	2.09
	WS-C1	West	Cyclonic	0.03	0.16	0.15	1.63	1.86	0.90	0.03	0.17	0.25	0.32	0.88	2.00
	WS-C2	West	Cyclonic	0.01	0.08	0.07	0.83	1.20	0.51	0.02	0.09	0.13	0.14	0.37	0.97

Table. S6: Main statistical details of the fifteen air mass types for PM_1 PMF factors (CS=Cold Season, WS=Warm Season, ST=Stagnant, A=Anticyclonic, C=Cyclonic) based on contribution (%).

Main season	Airmass type	Wind direction	Vorticity	Average mass contribution (%)											
				eBC-HOA	eBC-BBOA	eBC-CCOA	NO_3^-	SO_4^{-2}	NH_4^+	Cl^-	HOA	BBOA	CCOA	LO_OOA	MO_OOA
Winter	CS-ST	Stagnating	Anticyclonic	0	3	4	25	15	13	1	2	4	9	12	12
	CS-A1	East	Anticyclonic	0	2	7	19	18	12	1	2	4	14	9	12
	CS-A2	West	Anticyclonic	0	2	2	29	14	14	1	2	3	5	13	15
	CS-C1	South	Cyclonic	0	2	3	16	19	11	0	2	4	5	14	24
	CS-C2a	South West	Cyclonic	0	2	2	28	19	14	1	2	3	3	8	18
	CS-C2b	West	Cyclonic	0	2	2	14	29	10	1	3	3	4	11	21
Transition (Spring/ Fall)	TS-A1	North East	Anticyclonic	0	2	2	18	18	10	1	3	3	4	17	22
	TS-A2	West	Anticyclonic	0	2	1	26	18	13	1	2	3	3	10	21
	TS-C1	South West	Cyclonic	1	3	3	17	14	8	0	3	4	7	14	26
	TS-C2	North West	Cyclonic	0	2	2	27	18	14	1	2	3	4	10	17
Summer	WS-ST	Stagnating	Anticyclonic	1	1	2	11	21	8	0	3	4	4	12	32
	WS-A1	South East	Anticyclonic	0	2	4	19	19	11	1	2	3	8	13	18
	WS-A2	North West	Anticyclonic	0	2	2	23	17	12	1	2	2	5	12	22
	WS-C1	West	Cyclonic	0	0	2	19	22	11	0	2	3	4	11	24
	WS-C2	West	Cyclonic	0	2	2	19	27	11	1	2	3	3	8	22

References

Canonaco, F., Tobler, A., Chen, G., Sosedova, Y., Gates Slowik, J., Bozzetti, C., Rudolf Daellenbach, K., el Haddad, I., Crippa, M., Huang, R. J., Furger, M., Baltensperger, U., and Prévôt, A. S. H.: A new method for long-term source apportionment with time-dependent factor profiles and uncertainty assessment using SoFi Pro: Application to 1 year of organic aerosol data, Atmos. Meas. Tech., 14(2), 923–943, https://doi.org/10.5194/amt-14-923-2021, 2021.

Chen, G., Sosedova, Y., Canonaco, F., Fröhlich, R., Tobler, A., Vlachou, A., Daellenbach, K. R., Bozzetti, C., Hueglin, C., Graf, P., Baltensperger, U., Slowik, J. G., el Haddad, I., and Prévôt, A. S. H.: Time-dependent source apportionment of submicron organic aerosol for a rural site in an alpine valley using a rolling positive matrix factorisation (PMF) window, Atmos. Chem. Phys., 21(19), 15081–15101, https://doi.org/10.5194/acp-21-15081-2021, 2021.

Chen, G., Canonaco, F., Tobler, A., Aas, W., Alastuey, A., Allan, J., Atabakhsh, S., Aurela, M., Baltensperger, U., Bougiatioti, A., de Brito, J. F., Ceburnis, D., Chazeau, B., Chebaicheb, H., Daellenbach, K. R., Ehn, M., el Haddad, I., Eleftheriadis, K., Favez, O., Flentje, H., Font, A., Fossum, K., Freney, E., Gini, M., Green, D.C., Heikkinen, L., Herrmann, H., Kalogridis, A., Keernik, H., Lhotka, R., Lin, C., Lunder, C., Maasikmets, M., Manousakas, M.I., Marchand, N., Marin, C., Marmureanu, L., Mihalopoulos, N., Mocnika, G., Nęckia, J., O'Dowd, C., Ovadnevaite, J., Petera, T., Petita, J.E., Pikridasa, M., Matthew Platt, S., Pokorna, P., Poulain, L., Priestman, M., Riffault, V., Rinaldia, M., Rozanskia, K., Schwarz, J., Sciarea, J., Simon, L., Skiba, A., Slowik, J.G., Sosedova, Y., Stavroulas, I., Styszkoa, K., Teinemaa, E., Timonen, H., Tremper, A., Vasilescu, J., Via, M., Vodicka, P., Wiedensohler, A., Zografou, O., Cruz Minguillon, M., and Prévôt, A. S. H.: European aerosol phenomenology − 8: Harmonised source apportionment of organic aerosol using 22 Year-long ACSM/AMS datasets, Environment International, 166, https://doi.org/10.1016/j.envint.2022.107325, 2022.

Crippa, M., Canonaco, F., Lanz, V. A., Äijälä, M., Allan, J. D., Carbone, S., Capes, G., Ceburnis, D., Dall'Osto, M., Day, D. A., DeCarlo, P. F., Ehn, M., Eriksson, A., Freney, E., Ruiz, L. H., Hillamo, R., Jimenez, J. L., Junninen, H., Kiendler-Scharr, A., Kortelainen, A.-M., Kulmala, M., Laaksonen, A., Mensah10, A.A., Mohr1, C., Nemitz, E., O'Dowd, C., Ovadnevaite, J., Pandis, S. N., Petäjä, T., Poulain, L., Saarikoski, S., Sellegri, K., Swietlicki, E., Tiitta, P., Worsnop, D. R., Baltensperger, U., and Prévôt, A. S. H.: Organic aerosol components derived from 25 AMS data sets across Europe using a consistent ME-2 based source apportionment approach, Atmos. Chem. Phys., 14(12), 6159–6176, https://doi.org/10.5194/acp-14-6159-2014, 2014.

Crippa, M., Decarlo, P. F., Slowik, J. G., Mohr, C., Heringa, M. F., Chirico, R., Poulain, L., Freutel, F., Sciare, J., Cozic, J., di Marco, C. F., Elsasser, M., Nicolas, J. B., Marchand, N., Abidi, E., Wiedensohler, A., Drewnick, F., Schneider, J., Borrmann, S., Nemitz, E., Zimmermann, R., Jaffrezo, J.-L., Prevot, A. S. H., and Baltensperger, U. Wintertime aerosol chemical composition and source apportionment of the organic fraction in the metropolitan area of Paris, Atmos. Chem. Phys., 13(2), 961–981, https://doi.org/10.5194/acp-13-961-2013, 2013.

Dall'Osto, M., Ovadnevaite, J., Ceburnis, D., Martin, D., Healy, R. M., O'Connor, I. P., Kourtchev, I., Sodeau, J. R., Wenger, J. C., and O'Dowd, C.: Characterization of urban aerosol in Cork city (Ireland) using aerosol mass spectrometry, Atmos. Chem. Phys., 13(9), 4997–5015, https://doi.org/10.5194/acp-13-4997-2013, 2013.

Davison, A. C., and Hinkley, D. V.: Bootstrap methods and their application, Cambridge University Press, 1997.

Elser, M., Huang, R. J., Wolf, R., Slowik, J. G., Wang, Q., Canonaco, F., Li, G., Bozzetti, C., Daellenbach, K. R., Huang, Y., Zhang, R., Li, Z., Cao, J., Baltensperger, U., El-Haddad, I., and André, P.: New insights into PM2.5 chemical composition and sources in two major cities in China during extreme haze events using aerosol mass spectrometry, Atmos. Chem. Phys., 16(5), 3207–3225, https://doi.org/10.5194/acp-16-3207-2016, 2016.

Lin, C., Ceburnis, D., Hellebust, S., Buckley, P., Wenger, J., Canonaco, F., Prévôt, A. S. H., Huang, R. J., O'Dowd, C., and Ovadnevaite, J.: Characterization of Primary Organic Aerosol from Domestic Wood, Peat, and Coal Burning in Ireland, Environ. Sci. Technol., 51(18), 10624–10632, https://doi.org/10.1021/acs.est.7b01926, 2017.

Ng, N. L., Canagaratna, M. R., Jimenez, J. L., Zhang, Q., Ulbrich, I. M., and Worsnop, D. R.: Real-time methods for estimating organic component mass concentrations from aerosol mass spectrometer data, Environ. Sci. Technol., 45(3), 910–916. https://doi.org/10.1021/es102951k, 2011.

Ng, N. L., Canagaratna, M. R., Zhang, Q., Jimenez, J. L., Tian, J., Ulbrich, I. M., Kroll, J. H., Docherty, K. S., Chhabra, P. S., Bahreini, R., Murphy, S. M., Seinfeld, J. H., Hildebrandt, L., Donahue, N. M., Decarlo, P. F., Lanz, V. A., Prévôt, A. S. H., Dinar, E., Rudich, Y., and Worsnop, D. R.: Organic aerosol components observed in Northern Hemispheric datasets from Aerosol Mass Spectrometry, Atmos. Chem. Phys., 10(10), 4625–4641, https://doi.org/10.5194/acp-10-4625-2010, 2010.

Poulain, L., Spindler, G., Birmili, W., Plass-Dülmer, C., Wiedensohler, A., and Herrmann, H.: Seasonal and diurnal variations of particulate nitrate and organic matter at the IfT research station Melpitz, Atmos. Chem. Phys., 11(24), 12579–12599. https://doi.org/10.5194/acp-11-12579-2011, 2011.

van Pinxteren, D., Fomba, K. W., Spindler, G., Müller, K., Poulain, L., Iinuma, Y., Löschau, G., Hausmann, A., and Herrmann, H.: Regional air quality in Leipzig, Germany: Detailed source apportionment of size-resolved aerosol particles and comparison with the year 2000, Faraday Discussions, 189, 291–315, https://doi.org/10.1039/c5fd00228a, 2016.

van Pinxteren, D., Mothes, F., Spindler, G., Fomba, K. W., Cuesta, A., Tuch, T., Müller, T., Wiedensohler, A., and Herrmann, H.: Zusatzbelastung aus Holzheizung, Sächsisches Landesamt für Umwelt, Landwirtschaft und Geologie (LfULG), Dresden, https: //publikationen.sachsen.de/bdb/artikel/36106 TS33 , 2020.